CrystEngComm

PAPER

View Article Online
View Journal | View Issue

Cite this: *CrystEngComm*, 2014, **16**, 8363

O- vs. N-protonation of 1-dimethylaminonaphthalene-8-ketones: formation of a *peri* N–C bond or a hydrogen bond to the pi-electron density of a carbonyl group†

Nerea Mercadal,[a] Stephen P. Day,[b] Andrew Jarmyn,[a] Mateusz B. Pitak,[c] Simon J. Coles,[c] Claire Wilson,[d] Gregory J. Rees,[b] John V. Hanna*[b] and John D. Wallis*[a]

Received 10th May 2014,
Accepted 14th July 2014

DOI: 10.1039/c4ce00981a

www.rsc.org/crystengcomm

X-ray crystallography and solid-state NMR measurements show that protonation of a series of 1-dimethylaminonaphthalene-8-ketones leads either to *O* protonation with formation of a long N–C bond (1.637–1.669 Å) between *peri* groups, or to *N* protonation and formation of a hydrogen bond to the π surface of the carbonyl group, the latter occurring for the larger ketone groups (C(=O)R, R = *t*-butyl and phenyl). Solid state ^{15}N MAS NMR studies clearly differentiate the two series, with the former yielding significantly more deshielded resonances. This is accurately corroborated by DFT calculation of the relevant chemical shift parameters. In the parent ketones X-ray crystallography shows that the nitrogen lone pair is directed towards the carbonyl group in all cases.

Introduction

We are interested in mapping out the changes in electron distribution on the formation of a N–C bond *via* charge density measurements from X-ray diffraction studies on molecules containing N–C bonds of different lengths. Of particular interest are those bonds which are particularly long and thus represent bonds which are not fully formed. Bond formation is a fundamental process in chemistry, and its study underpins topics such as catalysis and enzyme action. The *peri*-naphthalene system has provided us with a series of zwitterionic materials such as **1–3** with N–C bonds in the range 1.612(2)–1.6536(14) Å,[1–3] significantly longer than a typical unperturbed N–C bond of *ca.* 1.47 Å. We have also recently reported the structures of two salts of the aldehyde **4** in which protonation on oxygen has been accompanied by bond formation between the *peri* dimethylamino and aldehyde groups to form cation **5** which has N–C bond lengths in the range 1.624(4)–1.638(2) Å.[3] A bond length as long as 1.71 Å has been reported in the tetrafluoroborate salt of the sterically hindered cation **6**.[4] We decided to investigate the structures of the salts formed from a series of naphthyl-8-ketones bearing a *peri*-dimethylamino group, **7–11**, in which the electronic properties and size of the ketone group is varied: from methyl to isopropyl to *t*-butyl, and also phenyl and trifluoromethyl. It was envisaged that protonation would take place on *O* with formation of a N–C bond between *peri* groups to give structures such as **12**, with the length of the new bond controlled by steric interactions between substituents at the terminal atoms of the bond. The resultant salts were studied by single X-ray crystallography, natural abundance solid state ^{1}H, ^{13}C and ^{15}N MAS NMR spectrometry and DFT calculations of the relevant corresponding NMR chemical shifts. The crystal structures of the five ketones **7–11** were also determined to see how the electronic and steric properties of the acyl group affected the interaction with the *peri*-dimethylamino group, following on from the original crystal structure determination of the methyl ketone **7**[5] by Dunitz *et al.*, which demonstrated that the dimethylamino group was oriented so that its lone pair of electrons could interact with the carbonyl group.

Discussion

Structures of ketones

The ketones **7–11** were prepared by *peri*-lithiation of 1-dimethylaminonaphthalene followed by treatment with the appropriate anhydride. For most cases, crystals of ketones were grown by slow evaporation of solutions and crystal structures measured by X-ray diffraction at low temperature.

[a] *School of Science and Technology, Nottingham Trent University, Clifton Lane, Nottingham NG11 8NS, UK. E-mail: john.wallis@ntu.ac.uk*
[b] *Department of Physics, University of Warwick, Coventry CV4 7AL, UK. E-mail: j.v.hanna@warwick.ac.uk*
[c] *UK National Crystallography Service, Chemistry, University of Southampton, Highfield Campus, Southampton, SO17 1BJ, UK. E-mail: S.J.Coles@soton.ac.uk*
[d] *Diamond Light Source Ltd, Harwell Science and Innovation Campus, Didcot, Oxfordshire, OX1 0DE, UK. E-mail: claire.wilson@diamond.ac.uk*

† Electronic supplementary information (ESI) available. CCDC 984760–984765, 984801–984806. For ESI and crystallographic data in CIF or other electronic format see DOI: 10.1039/c4ce00981a

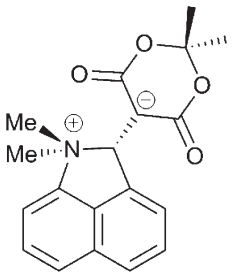

1

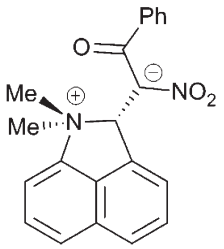

2

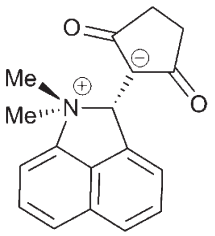

3

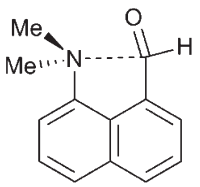

4

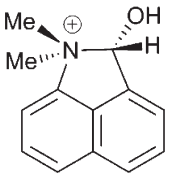

5

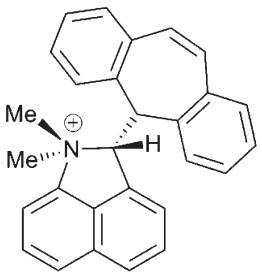

6

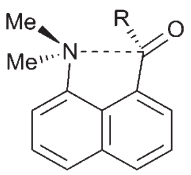

7 R = CH_3
8 R = $CH(CH_3)_2$
9 R = $C(CH_3)_3$
10 R = C_6H_5
11 R = CF_3

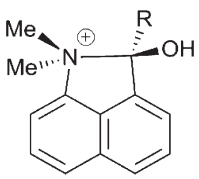

12

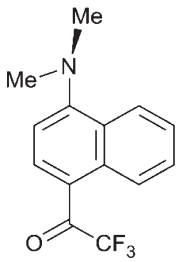

13

A very fine needle shaped crystal of the low melting isopropyl ketone **8** was grown by sublimation and was measured using synchrotron X-radiation. Details of the ketones' molecular geometries are summarised in Table 1, their molecular conformations are shown in Fig. 1 and their crystal packings provided in the ESI.† The molecular conformations of the five ketones are very similar, with each dimethylamino group adopting pyramidal geometry and the lone pair directed towards the carbonyl carbon of the ketone (Fig. 1). As the ketone group increases in size on going from methyl to isopropyl to *t*-butyl ketone, the N···C separation increases from 2.5290(13) in **7** to 2.613(7) in **8** to 2.6859(13) and 2.6649(14) Å in **9**. In the phenyl ketone **10** the N···C separation is similar to that in the methyl ketone, while the shortest N···C separation (2.424(2) Å) is in the most electron-deficient ketone which carries a trifluoromethyl group. The variation in this separation is achieved primarily by a change in the in-plane displacement of the ketone group. However, there is also an increasing displacement of the *peri* groups to either side of the naphthalene plane as the inter-group separation increases (Table 1).

Interestingly, for the *t*-butyl derivative, there are two independent molecules with similar $Me_2N\cdots C{=}O$ separations, but while one molecule shows the largest out of plane displacements for the N and C *peri*-substituent atoms in this series, the other molecule shows only minimal displacements. The similar N···C separation in the more planar form is realised by an increased outward splaying of the dimethylamino group and a widening of the external angle at the fusion between the two rings of the naphthalene framework. The overall optimisation of crystal packing in ketone **9** has led to the preference for adopting these two conformations, but illustrates the geometric consequences for the in-plane alignment of the two *peri* bonds. In all cases the carbonyl carbon atom is slightly pyramidalised with the carbon atom displaced towards the amino nitrogen atom by 0.072–0.125 Å (Table 1). While there is no clear trend, it is notable that the largest displacement is for the shortest N···C separation in the trifluoromethyl ketone. The dimethylamino groups are oriented such that the theoretical axes of their nitrogen atoms' lone pairs lie at 16–28° to their respective N···C vectors (Table 1), and for the two molecules of the *t*-butyl

Table 1 Selected molecular geometry for **7–11**[a]

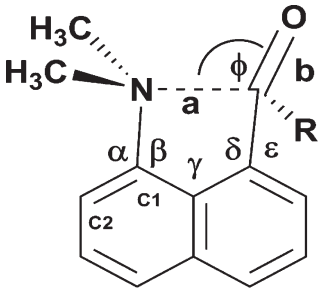

Compound, *R*	*a*/Å	*b*/Å	*ϕ*/°	τ_1/°[b]
7, CH_3	2.5290(13)	1.2196(13)	104.40(7)	80.48(13)
8, $CHMe_2$	2.613(7)	1.212(4)	106.13(19)	92.1(2)
9, CMe_3	2.6859(13)	1.2193(12)	101.58(6)	100.75(12)
	2.6649(14)	1.2165(12)	100.97(8)	84.18(12)
10, Ph	2.5376(19)	1.2200(17)	107.10(11)	83.70(19)
11, CF_3	2.424(2)	1.213(2)	107.26(12)	80.2(2)

Compound, *R*	τ_2/°[c]	*ΔC*/Å[d]	*Θ*/°[e]	*ΔN*p/Å N, C[f]
7, CH_3	−47.61(13)	0.0942(10)	16.4	+0.108(1), −0.093(1)
8, $CHMe_2$	−35.6(3)	0.075(3)	22.9	+0.202(2), −0.159(3)
9, CMe_3	−25.26(14)	0.0909(9)	28.1	+0.247(1), −0.308(1)
	−40.81(13)	0.0942(11)	27.0	+0.003(1), −0.021(1)
10, Ph	−46.3(2)	0.0722(14)	17.1	+0.151(1), −0.113(1)
11, CF_3	−45.3(2)	0.1252(16)	20.4	+0.049(1), +0.010(2)

[a] Ranges for angles: *α*: 122.39(4)–124.23(16)°; *β*: 115.35(16)–117.66(9)°; *γ*: 121.15(13)–123.56(9)°; *δ*: 121.51(15)–124.83(8)°; *ε*: 115.49(9)–118.13(17)°, further details in ESI. [b] τ_1: torsion: C2–C1–N1–C(H_3), *cis* to C═O. [c] τ_2: torsion: C2–C1–N1–C(H_3), *trans* to C═O. [d] *ΔC*: deviation of C(═O) atom from the plane of its three neighbouring atoms towards N(Me_2). [e] *Θ*: angle between N···C vector and theoretical N lone pair axis. [f] *ΔN*p: deviation of *peri* atoms, N(Me_2) and C(═O), from naphthalene ring's best plane.

derivative the groups have maintained almost the same relative orientations. In contrast, when the substituents are oriented *para* rather than *peri* as in **13**, an isomer of ketone **11**, structural studies show strong interaction between substituents through the aromatic ring, and not through space. Further details are in the ESI.†

Preparation of salts of ketones 7–11

Treatment of ether solutions of ketones **7–11** with an ether solution of one of the acids, HCl, HBF_4 or CF_3SO_3H, led to the precipitation of the corresponding salts. For each ketone, the most crystalline salts were studied by X-ray diffraction and natural abundance SS-NMR. The salts studied were: for **7** the hydrated chloride salt and the triflate salt, for **8** the BF_4 salt, for **9** the triflate salt, for **10** the BF_4 salt and for **11** a hydrated triflate salt. X-ray diffraction studies showed that the salts from ketones **7**, **8** and **11** involved addition of the dimethylamino group to the protonated carbonyl group, whereas the salts from the *t*-butyl and phenyl ketones **9** and **10** are protonated on the dimethylamino group and there is a hydrogen bond between the N–H of the cation and the pi surface of the carbonyl group. The ^{15}N SS-NMR studies identified a distinct difference of *ca.* 50 ppm in the chemical shift for the two series of compounds. The ^{13}C SS-NMR spectra allowed identification of the carbonyl carbon resonance in the latter series of salts. The results are described in more detail below.

Crystal structures of *O*-protonated salts of cations 7-H^+, 8-H^+ and 11-H^+

The crystal structure of the four salts 7-H^+·Cl^-·H_2O, 7-H^+·$CF_3SO_3^-$, 8-H^+·BF_4^- and 11-H^+·$CF_3SO_3^-$·H_2O involve formation of a bond between the *peri* groups and hydrogen bonding of the counter-ion or a molecule of water to the cation's hydroxyl group. The structures are shown in Fig. 2–4, and selected molecular geometry is given in Table 2. In the hydrated chloride salt of cation 7-H^+ the chloride ion forms a hydrogen bond to the hydroxyl group of a cation (OH···Cl^-: 2.17(3) Å), and chlorides are linked together with bridging water molecules (OH···Cl^-: 2.41 & 2.48 Å) to form Cl^-···H–O–H···Cl^- chains along the *c* axis (Fig. 2). In contrast, the salts of 7-H^+ with triflate and 8-H^+ with tetrafluoroborate are not hydrated and there are just OH···$[O–SO_2CF_3]^-$ and OH···$[F-BF_3]^-$ hydrogen bonds between cation and anion (1.80(8) and 1.82(3) Å respectively) (Fig. 2). In the triflate salt of 11-H^+ a water molecule makes a hydrogen bond to the cation's hydroxyl group (OH···OH_2: 1.68(2) Å), and then two such water molecules and two triflate ions form a cyclic hydrogen bonded motif (H–O–H···O–SO_2CF_3: 1.893(5) and 1.946(6) Å) (Fig. 3). Interestingly, the crystal packing segregates the trifluoromethyl groups from cations and anions away from the rest of the hydrocarbon based moieties (Fig. 4). The bond between the *peri* groups for the methyl and isopropyl ketone salts are remarkably long: 1.669(2), 1.6709(6) and 1.662(2) Å,

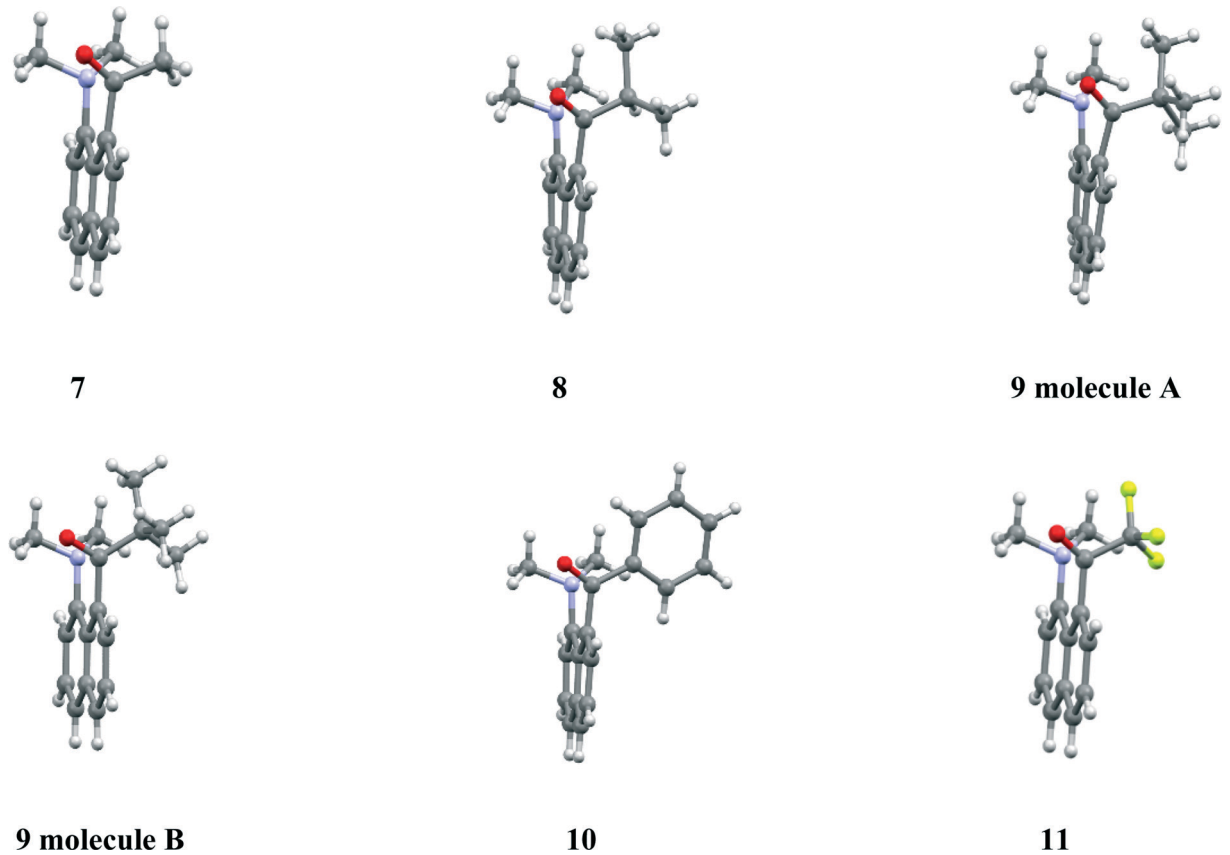

Fig. 1 Molecular structures of the ketones **7**–**11**, showing the increase in displacements from the naphthalene plane as the $Me_2N\cdots C{=}O$ separation increases (top row), but the second molecule of **9** (bottom, left) shows minimal such displacements. The shortest $Me_2N\cdots C{=}O$ separation is in the trifluoromethyl ketone **11**.

and longer than for the aldehyde salt **5** (1.624(4)–1.638(2) Å). The salt from the more electron deficient trifluoromethyl ketone has the shortest N–C bond, 1.6375(18) Å.

The room temperature crystal structure of the trifluoroacetate salt of methyl ketone **7** has been reported,[6] and shows the same type of *O*-protonated cation structure with a bond length of 1.679 Å between *peri* groups. Increased steric pressure between the *N*-methyl and C-isopropyl groups in **8**-H^+ compared to the corresponding interaction between two methyl groups in **7**-H^+ is relieved in part by an increase of the torsion about the *peri*-bond (from 23.6° to 30.8°) and by the greater length of the C–$CHMe_2$ bond of 1.541(3) Å compared to 1.513(2) Å in **7**-H^+.

In **11**-H^+ the shorter bond between *peri* groups is accompanied by a long C–CF_3 bond of 1.5452(19) Å so that the shortest intramolecular H···F contacts with an *N*-methyl group are 2.36 and 2.51 Å. For the ketones with *t*-butyl and phenyl groups, rather than form cyclised materials, protonation on the N atom is preferred. For the former, the N–C bond which would be formed in *O*-protonation mode would have to be longer and weaker than in **7**-H^+ and **8**-H^+, due to steric pressure from the *t*-butyl group, while for the latter, the carbonyl group is stabilised by conjugation with the phenyl group.

Crystal structures of *N*-protonated salts of cations **9**-H^+ and **10**-H^+

The crystal structures of salts **9**-$H^+\cdot CF_3SO_3^-$ and **10**-$H^+\cdot BF_4^-$ show a cation formed by *N*-protonation with a hydrogen bond to the *peri* ketone group. There are two crystallographically unique cations and anions in the *t*-butyl ketone salt. The structures are shown in Fig. 5, with details of their geometries in Table 3. The relative orientations of the *peri* groups in all three cations are similar, and the hydrogen bonds between the protonated dimethylamino group and the carbonyl O atom lie in the range 1.77(2)–1.80(3) Å. The bond angle at the H atom lies in the narrow range 156(2)–159(2)°, and the angle at the O atom is in the range 98.6(8)–103.6(8)°. This is achieved by the carbonyl and N–H groups being directed to the same side of the naphthalene ring and then tilting towards each other. The two *peri* groups have to be splayed apart in the naphthalene plane, though this is limited by interactions with the *ortho* H atoms. The ketone is splayed out further than the dimethylammonium group; for the two unique molecules of **9**-H^+ the *t*-butyl group makes two (butyl)H···*ortho* H contacts as short as 2.08–2.11 Å, and one *N*-methyl group makes a H···H contact with its *ortho* H atom also in the same range. In **10**-H^+ the in-plane steric pressure from *ortho*-H atoms in less and only the *N*-methyl

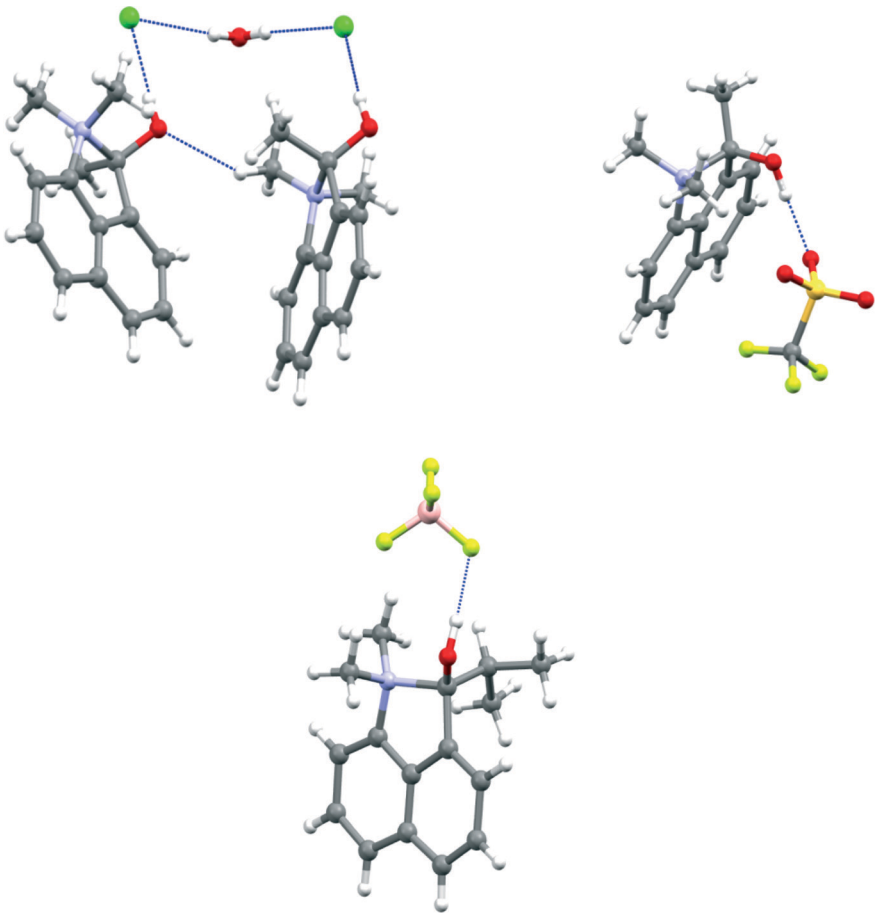

Fig. 2 Molecular structures of (a) the hydrated chloride salt of the *O*-protonated methyl ketone **7**-H^+ showing the involvement of anions and water molecules in the hydrogen bonding pattern (left), (b) the triflate salt of **7**-H^+ (right) and (c) the tetrafluoroborate salt of the *O*-protonated isopropyl ketone **8**-H^+ (below).

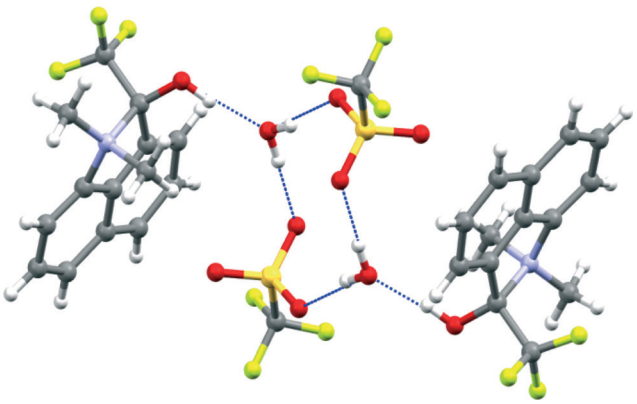

Fig. 3 Hydrogen bonding linking together two cations with a cluster of two triflate anions and two water molecules in the crystal structure of **11**-H^+·triflate·H_2O.

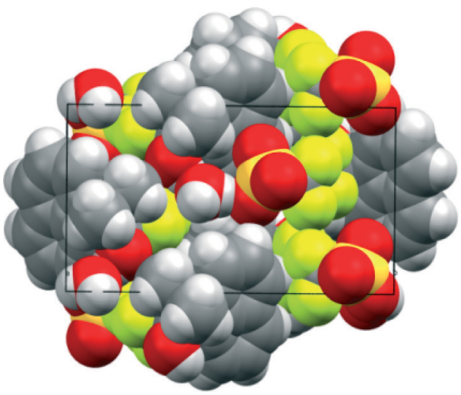

Fig. 4 Space-filling view of the crystal packing of **11**-H^+·triflate·H_2O viewed down the *a* axis, showing the segregation of the fluorous residues.

group makes a short H···H contact (2.16 Å). The naphthalene ring system is not strongly distorted from planarity and the *peri* substituent N and C atoms lie close to this plane; the largest deviations are for the *peri* C atoms in the two cations of **9**-H^+ (by 0.2–0.3 Å) which act to reduce steric pressure between the *t*-butyl group and an *ortho* H atom.

With regard to the hydrogen bonding in these two salts, the restrictions imposed by the *peri* groups lead to the

Table 2 Selected molecular geometry for *O*-protonated salts of ketones **7**, **8** and **11**[a]

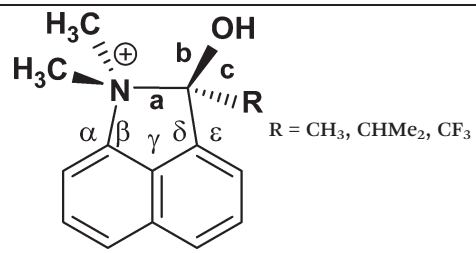

R = CH_3, $CHMe_2$, CF_3

Salt	*a*/Å	*b*/Å	N–Me/Å	*c*/Å
7-H^+·Cl^-·H_2O	1.669(2)	1.364(2)	1.497(2) & 1.503(2)	1.513(2)
7-H^+·$CF_3SO_3^-$	1.670(6)	1.415(6)	1.490(5) & 1.511(6)	1.482(6)
8-H^+·BF_4^-	1.662(2)	1.367(2)	1.507(2) & 1.497(2)	1.541(3)
11-H^+·$CF_3SO_3^-$·H_2O	1.6375(18)	1.3476(13)	1.5037(18) & 1.5124(18)	1.5452(19)

[a] Ranges for angles: *α*: 128.6(4)–129.49(17)°; *β*: 107.92(16)–109.3(3)°; *γ*: 113.6(4)–113.91(15)°; *δ*: 108.91(15)–109.95(14)°; *ε*: 130.39(16)–131.33(13)°, further details in ESI.

H atom lying to one side of the carbonyl group, by 1.35–1.50 Å, and to the C(naphthalene)–C═O···H torsion angle lying in the range 53.2(8)–61.5(8)°. This is very different from the preferred hydrogen bonding geometry to a carbonyl group in which the H atom lies in the carbonyl plane, out beyond the O atom, and with a C═O···H angle in the range 110–180°.[7] Thus, these structures provide a very nice model for hydrogen bonding to the underside of a carbonyl group, *i.e.* to the pi electron density rather than lone pair density. This is of particular interest given the proposal that hydrogen bonding to the pi surface of a carbonyl group promotes the kinetics of deprotonation *alpha* to the carbonyl group in various enzyme active sites.[8] Hydrogen bonding from ammonium and substituted ammonium ions to the pi faces of alkenes, alkynes and benzene rings is well known.[9,10] The energy of interaction of a $N^{(+)}$–H bond with ethene has been estimated at *ca.* 10 kcal mol^{-1}.[10]

In the solution NMR spectra for the salts of **9**-H^+ and **10**-H^+ the N–H group gives signals at δ_H 11.15 and 11.27 ppm respectively, and the carbonyl carbon atoms resonate at δ_C 221.3 and 205.0 ppm which are *ca.* 8 ppm downfield from the positions observed in the parent ketones (**9**: 213.0 and **10**: 193.5 ppm) consistent with these salts retaining their *N*-protonated structures in solution. Solution NMR studies of the salts of 7-H^+, **8**-H^+ and **11**-H^+ suggest that the closed ring structure is maintained in solution for the salts of the methyl and trifluoromethyl ketones, 7-H^+·Cl (in CD_3OD) and 7-H^+·triflate and **11**-H^+·triflate (in $(CD_3)_2CO$), with the carbon atom attached to the hydroxyl and ammonium groups appearing at δ_C 124.8 and 122.5 ppm in the salts of the methyl ketone. In contrast, the salt of the more hindered isopropyl ketone exists in CD_3CN as a 6.5 : 1 mixture of *N*-protonated to *O*-protonated forms, *i.e.* favouring

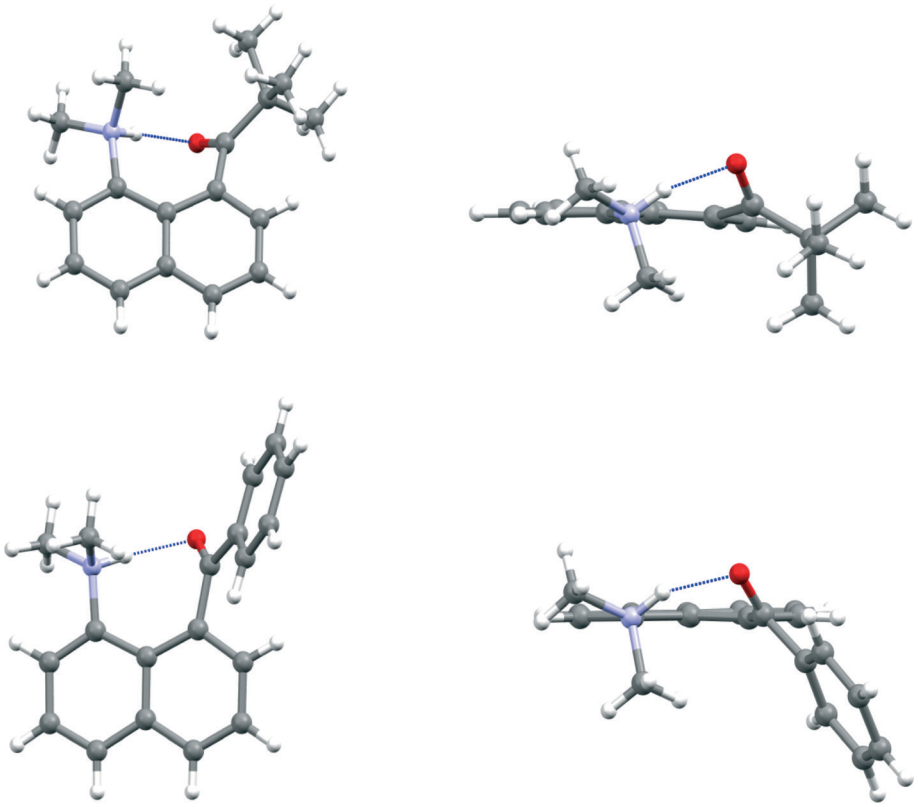

Fig. 5 Two views of the molecular structure and intramolecular hydrogen bond of (a) one of the two independent cations of **9**-H^+ (top), (b) the cation **10**-H^+ (bottom).

Table 3 Selected molecular geometry for *N*-protonated salts of ketones **9** and **10**[a]

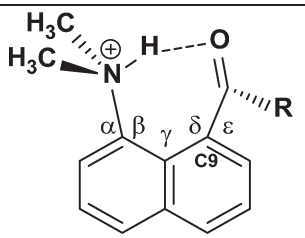

Salt	C═O/Å	O···N/Å	NH···O/Å	N–H···O/°
9-$H^+\cdot CF_3SO_3^-$	1.226(2)	2.641(2)	1.77(2)	159(2)
10-$H^+\cdot BF_4^-$	1.233(2)	2.658(3)	1.78(3)	157(2)
	1.229(3)	2.660(3)	1.80(3)	156(2)

Salt	τ/°[b]	C═O···H/°
9-$H^+\cdot CF_3SO_3^-$	53.2(8)	103.6(8)
10-$H^+\cdot BF_4^-$	61.5(8)	101.2(7)
	56.5(9)	98.6(8)

[a] Ranges for angles: α: 116.17(19)–118.0(2)°; β: 119.6(2)–121.02(17)°; γ: 128.4(2)–129.41(18)°; δ: 124.47(18)–25.8(2)°; ε: 114.0(2)–114.87(19)°, further details in ESI. [b] τ = C9–C═O···H.

the form not observed in the solid state, with the major species exhibiting a N–H resonance at δ_H 12.45 ppm and a carbonyl carbon resonance at δ_C 217.3 ppm. The balance between the two structural forms, in this case at least, is fine and dependent on the particular external environment, with the form observed in the solid state controlled by the relative stabilities of the crystal packing arrangements.

Solid state NMR studies

The two sets of salts whose X-ray structures showed either ring formation with *O*-protonation or just *N*-protonation were studied by solid state ^{1}H, ^{13}C and ^{15}N MAS NMR, to establish a method for determining between the two species, since as observed for **8**-$H^+\cdot BF_4$ the structure adopted in solution may be different. The measured ^{15}N data are particularly diagnostic in discriminating between the two types of structures. The ^{15}N CPMAS NMR data are shown in Fig. 6 and Table 4, and it can be observed that the ^{15}N δ_{iso} values are highly correlated around two regions: δ_{iso} −334.6 and −334.5 ppm (for **9**-$H^+\cdot CF_3SO_3^-$, **10**-$H^+\cdot BF_4^-$, respectively) and the more deshielded region of δ_{iso} −284.0 to −285.6 ppm (for **7**-$H^+\cdot Cl^-\cdot H_2O$, **7**-$H^+\cdot CF_3SO_3^-$ and **11**-$H^+\cdot CF_3SO_3^-\cdot H_2O$). This observation unambiguously demonstrates the existence of two distinct N environments within this series. The chemical shifts of the latter group of salts is similar to that of the cation **5** formed by intramolecular attack of the dimethylamino group on a protonated aldehyde group (δ_{iso} −290 ppm)[3] also determined by ^{15}N MAS NMR methods. Previous studies have reported that solid trimethylammonium chloride, which exhibits moderately strong N–H···Cl hydrogen bonding, has a ^{15}N shift of δ_{iso} −335.7 ppm for the $(CH_3)_3NH^+$ cation.[11] This has a comparable N environment to that of the *N*-protonated cations in **9**-$H^+\cdot CF_3SO_3^-$, **10**-$H^+\cdot BF_4^-$, and this is reflected by the similar ^{15}N δ_{iso} values (with small variations in δ_{iso} evident due to the difference in the electronegativity of the hydrogen bond acceptor). In contrast, the considerable downfield shift observed in the cations **7**-$H^+\cdot Cl^-\cdot H_2O$, **7**-$H^+\cdot CF_3SO_3^-$ and **11**-$H^+\cdot CF_3SO_3^-\cdot H_2O$ is due primarily to the electron withdrawing effect of the OH group. For comparison, the reported ^{15}N isotropic chemical shift for solid tetramethylammonium iodide is δ_{iso} −342.2,[12] but even for a neutral N atom in 2,2-dimethyl-1,3-oxazolidine, which contains an α-O atom, the ^{15}N chemical shift occurs at δ_{iso} −305–−316 ppm.[13] The additional positive charge of cations **7**-H^+ and **11**-H^+ contributes to their further downfield shifts. Interestingly, the ^{15}N chemical shifts of cations **7**-H^+ and **11**-H^+ are closer to that in *N*,*N*-dimethylacetamide (δ_{iso}(solution) −282.2 ppm)[14] in which the N lone pair is partially donated to a carbonyl group.

The ^{15}N chemical shift parameters calculated *via* the GIPAW approach (see Table 4) closely mirror this observed demarcation in the δ_{iso} values according to the structural motif describing each system. The crystal structure data for **9**-$H^+\cdot CF_3SO_3^-$ and **10**-$H^+\cdot BF_4^-$ suggest that there is protonation of the N site in these structures, and the implicit hydrogen bond remains after allowing the crystal structures to relax. This provides supporting evidence that the π-hydrogen bond arrangement in these particular systems is stable. As observed in Table 4, although the data trends are unambiguously reflected in the CASTEP data, the calculated ^{15}N δ_{iso} values consistently represent a high field/lower frequency overestimation even after the dispersion correction is applied. The combined structure relaxation/dispersion correction (SEDC) approach only marginally improves the correlation between the measured and calculated ^{15}N δ_{iso} data, with the shift differences for the hydrogen bonded systems being typically $\Delta\delta_{iso}$ ~10 ppm, whereas for the directly bonded systems it amounts to $\Delta\delta_{iso}$ ~0.5–5 ppm.

The ^{13}C CPMAS NMR data are also displayed in Fig. 6 with the measured ^{13}C δ_{iso} values summarized in Table 4. For the internally hydrogen bonded **9**-$H^+\cdot CF_3SO_3^-$ and **10**-$H^+\cdot BF_4^-$ systems the corresponding ketone moiety is evidenced by the ^{13}C shifts at δ_{iso} 221.2 and 201.3 ppm, respectively, which are very similar to those observed in their solution spectra. The large ^{13}C shift difference of $\Delta\delta_{iso}$ ~20 ppm exhibited between the ketone C atoms reflects the differences in electron donation and bond strength between the pendant Ph and $C(CH_3)_3$ groups and the C═O moiety. Of note is that these chemical shifts are 8.2 and 7.7 ppm downfield, respectively, from the carbonyl carbon signals observed in the solution spectra of the unprotonated ketones, suggesting an effect from the formation of the hydrogen bond to a positively charged group.

In contrast, for cations in **7**-$H^+\cdot Cl^-\cdot H_2O$, **7**-$H^+\cdot CF_3SO_3^-$ and **11**-$H^+\cdot CF_3SO_3^-\cdot H_2O$ the addition of the dimethylamino group to the protonated ketone group leads to a long N^+–C(OH)R bond where the resultant quaternary C has ^{13}C shifts in the range δ_{iso} 127–136 ppm; this phenomenon has been outlined by previous studies.[3,15–17] In a similar fashion to the

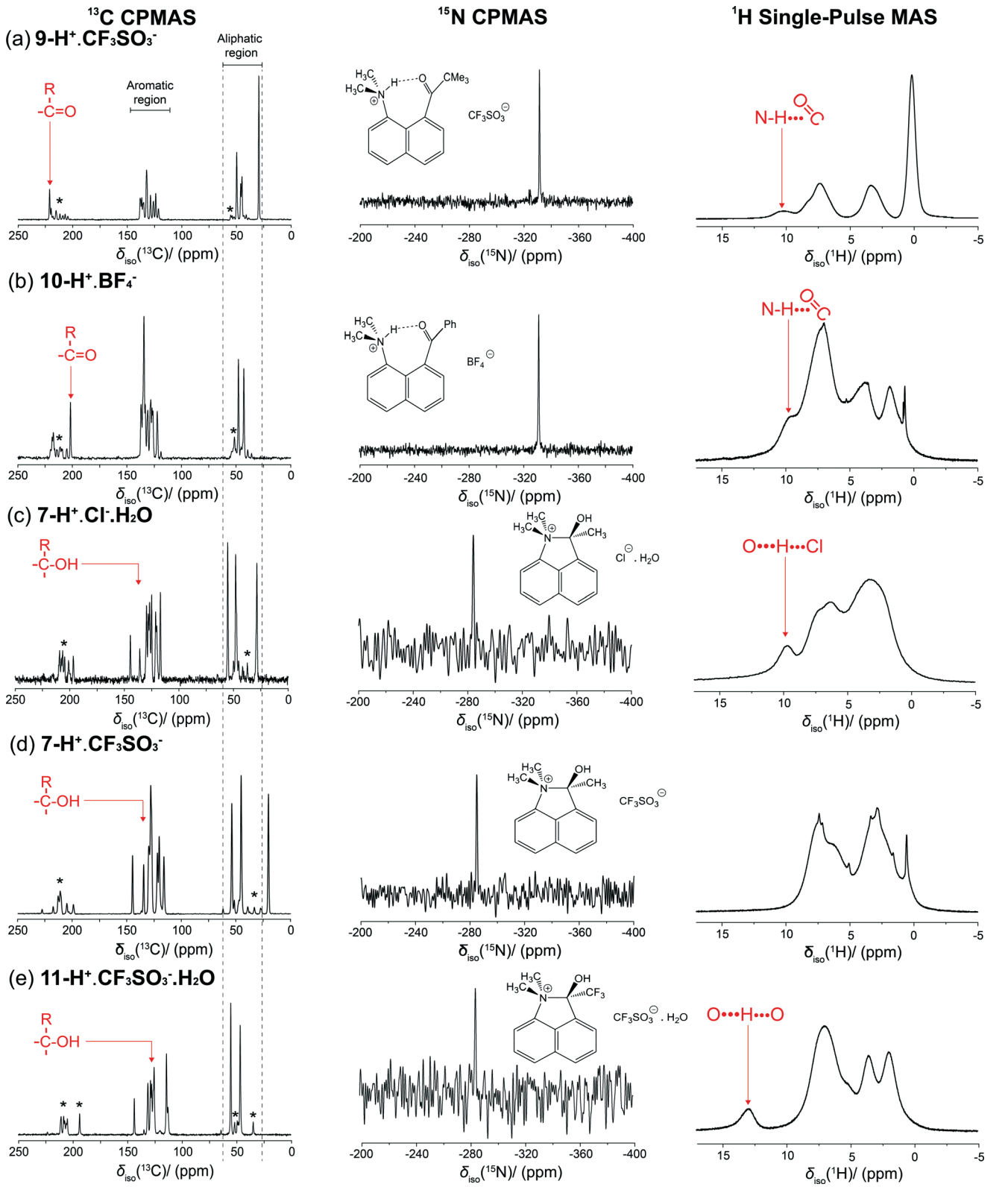

Fig. 6 ^{13}C, ^{15}N and ^{1}H CPMAS NMR spectra for salts **9**-$H^+ \cdot CF_3SO_3^-$ and **10**-$H^+ \cdot BF_4^-$ (upper) and the salts **7**-$H^+ \cdot Cl^- \cdot H_2O$, **7**-$H^+ \cdot CF_3SO_3^-$ and **11**-$H^+ \cdot CF_3SO_3^- \cdot H_2O$ (lower). * represent the spinning sidebands.

^{15}N study, the corresponding DFT calculated ^{13}C δ_{iso} parameters corroborate the demarcation between the hydrogen bonded and directly bonded systems; however, in contrast to the ^{15}N study, the CASTEP calculations supported by only the

Table 4 Experimental and calculated parameters from solid-state ^{15}N, ^{13}C and ^{1}H NMR studies

^{15}N	Experiment $\delta_{iso,mas}$ (ppm)(±0.5)	CASTEP/PBE δ_{iso} (ppm)	CASTEP/SEDC δ_{iso} (ppm)
9-$H^+\cdot CF_3SO_3^-$	−334.7	−344.9	−344.3
10-$H^+\cdot BF_4^-$	−334.5	−345.2	−345.0
7-$H^+\cdot Cl^-\cdot H_2O$	−284.0	−290.3	−288.9
7-$H^+\cdot CF_3SO_3^-$	−284.8	−289.9	−288.0
11-$H^+\cdot CF_3SO_3^-\cdot H_2O$	−285.6	−288.3	−286.0
^{13}C	Experiment $\delta_{iso,mas}$ (ppm)(±0.5)	CASTEP/PBE δ_{iso} (ppm)	CASTEP/SEDC δ_{iso} (ppm)
9-$H^+\cdot CF_3SO_3^-$	201.3	205.3	206.5
10-$H^+\cdot BF_4^-$	221.2	229.8	230.2
7-$H^+\cdot Cl^-\cdot H_2O$	136.0[a]	136.6	138.3
7-$H^+\cdot CF_3SO_3^-$	134.8[a]	136.3	139.8
11-$H^+\cdot CF_3SO_3^-\cdot H_2O$	127.7[a]	127.2	130.0
^{1}H	Experiment $\delta_{iso,mas}$ (ppm)(±0.5)	CASTEP/PBE δ_{iso} (ppm)	CASTEP/SEDC δ_{iso} (ppm)
9-$H^+\cdot CF_3SO_3^-$	9.6	10.3	9.9
10-$H^+\cdot BF_4^-$	10.2	10.7	10.6
7-$H^+\cdot Cl^-\cdot H_2O$	10.1	9.9	9.9
7-$H^+\cdot CF_3SO_3^-$	7.3	7.9	7.9
11-$H^+\cdot CF_3SO_3^-\cdot H_2O$	12.9	15.1	15.5

[a] Tentative assignments based on the predicted shifts obtained from the GIPAW CASTEP calculation.

PBE functional give a superior correlation with the experimentally measured ^{13}C CPMAS data in comparison to those undertaken with the SEDC scheme. From Table 4 it is evident that the SEDC scheme causes a divergence away from the PBE supported (and experimental) shifts by a factor of δ_{iso} ~1–3 ppm.

Previous computational and experimental studies of carbonyl and (in particular) carboxylic systems have shown that a shift to higher δ_{iso} values has largely been attributed to a strong dependence of the δ_{22} component of the second rank chemical shift anisotropy (CSA) tensor.[16–19] In the principal axis frame of this tensor the δ_{22} component is aligned along the C═O bond and is highly correlated to the overall strength of the hydrogen bond.[18] It is worth noting that the GIPAW DFT calculations underpinning this work predict a similar alignment of the δ_{22} component of the CSA tensor along the C═O bond in the ketone moiety for the **9**-$H^+\cdot CF_3SO_3^-$ and **10**-$H^+\cdot BF_4^-$ salts suggesting that the large δ_{iso} values ($\delta_{iso} > 200$ ppm) originate from the dominant contribution of the δ_{22} component of the CSA tensor; this phenomenon is particularly prevalent for the **10**-$H^+\cdot BF_4^-$ system. These DFT calculations also demonstrate that there is very little variation in the magnitude of δ_{33}, as similarly observed in other studies.[17–19]

The ^{1}H MAS NMR data acquired under single pulse conditions are also shown in Fig. 6. Generally, the ^{1}H δ_{iso} value is a very direct entity for identifying and gauging the strength of hydrogen bonding as the extent to which the proton is deshielded correlates directly with the downfield shift in the ^{1}H resonance. The ^{1}H MAS spectra for **9**-$H^+\cdot CF_3SO_3^-$ and **10**-$H^+\cdot BF_4^-$ show resonances located at δ_{iso} 9.5 and 10.3 ppm, respectively, that can be considered as representing weak hydrogen bonding. In solution the corresponding signals are δ_H 11.1–11.3 ppm. For the cyclised cations studied, only the hydrated **11**-$H^+\cdot CF_3SO_3^-\cdot H_2O$ salt exhibits a characteristic downfield ^{1}H signal at δ_{iso} ~13 ppm. This salt contains three hydrogen bonds, two between triflates and water (1.89 and 1.95 Å) and a shorter one (1.68 Å) between the cation's OH group and the water. For the hydrated chloride salt **7**-$H^+\cdot Cl^-\cdot H_2O$, with a OH–Cl^- hydrogen bond and two hydrogen bonds between chloride and water, a resonance is observed at ~10 ppm, while for the corresponding triflate salt the signal is probably obscured by aromatic hydrogen signals. In all cases studied here, none correspond to particularly strong hydrogen bonding for which the ^{1}H MAS NMR signal would be expected to be in the δ_{iso} 16–22 ppm range.[17,19,20]

From Table 4 a comparison of the experimental and DFT calculated ^{1}H δ_{iso} values shows that CASTEP has again overestimated these shifts on the downfield side, even after the Semi-Empirical Dispersion Correction (SEDC) scheme is applied. As the extent of the downfield shift correlates with the strength of the hydrogen bond CASTEP appears to be consistently predicting slightly stronger hydrogen bonds than those observed experimentally. Conventionally, the greatest errors in the δ_{iso} calculations are found in those systems where hydrogen bonding has a more dominant role in the structural formation, which is consistent with CASTEP's inexact treatment of van der Waals' forces. However, given that the application of the SEDC scheme does not improve the results significantly this error is likely to be due to a systematic error originating from the condition of 0 K imposed on atomic positions for the calculations. Unaccounted for motional atomic effects due to thermal fluctuations (particularly of the hydrogen bonding proton) could be observed as an average nuclear environment with a weaker hydrogen bond in the NMR experiment.

Conclusion

X-ray crystallography and SS-NMR provide a powerful combination of techniques for studying the protonated salts of a series of 1-dimethylamino-naphthalenes with *peri* ketone groups, and have provided interesting structural models for incomplete bond formation between the two groups and for hydrogen bonding between a protonated dimethylamino group and the pi face of the carbonyl group. Three of the salts provide some of the longest N–C bonds known, and further insight into these incompletely formed N–C bonds will come from charge density measurements. The hydrogen bonding to the side of a carbonyl group, rather than to its terminal lone pairs, is an aspect which is not often considered in crystal engineering. It is of interest to see whether formation of attractive interactions or covalent bonds between functional groups could be used as a method for organising molecules in the solid-state.

Experimental

Preparation of ketones

n-BuLi (18.7 ml, 2.5 M in hexane solution) was added to a stirred solution of 1-dimethylaminonaphthalene (2.00 g, 11.7 mmol) in dry ether (30 ml) under nitrogen at room temperature and left for 4 days during which time a yellow precipitate formed. The solution was carefully removed, and the yellow solid washed several times with dry ether under nitrogen. The solid was suspended in dry ether (30 ml), cooled to −78 °C and a solution of the appropriate acid anhydride (15 mmol) in dry ether (20 ml) added. The mixture was allowed to gradually warm to room temperature over 12 h, after which it was treated with methanol (30 ml) and the solvent evaporated. The residue was extracted with dichloromethane (2 × 50 ml), and the combined extracts washed with water (2 × 50 ml) and brine (1 × 50 ml) and then dried with anhydrous magnesium sulphate. Evaporation gave the crude product which was purified further by column chromatography with cyclohexane–ethyl acetate mixtures. Full characterisations of the products **7**–**11** are given in the ESI.† Products **8**, **9** and **13** have been described before.[21,22]

Preparation of salts

A stirred solution of the ketone (2 mmol) in dry ether (20 ml) under nitrogen was treated with a *ca.* 1 M solution of the acid (HCl, HBF_4 or CF_3SO_3H) (2.5 mmol) in dry ether at room temperature to give a precipitate. After stirring for 30 min, the solid was filtered off, washed with ether and dried under vacuum to give the salt. Full characterisations of the salts **7**-$H^+\cdot Cl^-\cdot H_2O$, **7**-$H^+\cdot CF_3SO_3^-$, **8**-$H^+\cdot BF_4^-$, **9**-$H^+\cdot CF_3SO_3^-$, **10**-$H^+\cdot BF_4^-$ and **11**-$H^+\cdot CF_3SO_3^-\cdot H_2O$ are given in the ESI.†

X-ray crystallography

Low temperature (100–150 K) X-ray diffraction data (Mo Kα) for compounds **7**, **9**, **9**-$H^+\cdot CF_3SO_3^-$ and **11**-$H^+\cdot CF_3SO_3^-$ were collected at the UK National Crystallography Centre,[23] Southampton University on a Rigaku AFC12 diffractometer equipped with enhanced sensitivity (HG) Saturn724+ CCD detector mounted at the window of an FR-E+ *SuperBright* rotating anode generator (Mo Kα, λ = 0.71075 Å) with VHF *Varimax* optics (70 μm focus) using Crystal Clear software[24] for data collection and reduction. For compounds **10**, **11**, **14**, **7**-$H^+\cdot Cl^-\cdot H_2O$, **7**-$H^+\cdot CF_3SO_3^-$, **8**-$H^+\cdot BF_4^-$, **10**-$H^+\cdot BF_4^-$ data were measured on an Agilent Xcalibur diffractometer equipped with a Sapphire detector at Nottingham Trent University using the CrysAlis-Pro software package.[25] Diffraction data for **8** was performed with the use of synchrotron X-rays at Diamond Light Source UK,[23] beamline I19 (λ = 0.6889 Å) on a Crystal Logic diffractometer and Rigaku Saturn 724+ detector equipped with an Oxford Cryosystems Cryostream and using Crystal Clear software.[24] Structures were solved are refined using the SHELXS and SHELXL suite of programs[26] using the XSEED interface.[27] Molecular illustrations were made with Mercury.[28] Crystal data are provided in Tables 5 and 6. Data is deposited at the Cambridge Crystallographic Data Centre with code numbers CCDC-984760–984765 and 984801–984806.

^1H, ^{13}C and ^{15}N MAS NMR measurements

Natural abundance solid state ^{13}C and ^{15}N MAS NMR measurements were performed at 14.1 and 11.7 T, respectively, using a Bruker Avance II+ −600 spectrometer (Larmor frequencies of $\nu_0(^1H)$ = 600.3 MHz and $\nu_0(^{13}C)$ = 150.9 MHz) and a Bruker Avance III-500 spectrometer (Larmor frequencies of $\nu_0(^1H)$ = 500.3 MHz and $\nu_0(^{13}C)$ = 50.7 MHz). All data were acquired at ambient temperatures. The ^{15}N measurements were performed using a ramped ^1H–^{15}N cross-polarisation MAS (CPMAS) NMR experiment using a Bruker 3.2 mm triple channel (HXY) MAS probe operating at a spinning frequency of 12 kHz. The SPINAL-64 heteronuclear decoupling scheme was used during acquisition with a ^1H decoupling field of $\nu_1(^1H)$ = 100.0 kHz being implemented. A minimum of 14 000 transients were acquired for each spectrum, and an initial ^1H $\pi/2$ pulse of 2.5 μs, a ^1H–^{15}N Hartmann–Hahn contact period of 1.0 ms and a recycle delay of 5.0 s were utilised in all ^{15}N CPMAS NMR measurements. All ^{15}N CPMAS NMR data were calibrated against the primary ^{15}N reference of CH_3NO_2 in $CHCl_3$ *via* a secondary solid reference of ^{15}N labelled histidine (three ^{15}N shifts of δ_{iso} −333.1, −204.3 and −191.0 ppm), which was also used to establish the ^1H–^{15}N Hartmann–Hahn match condition. The corresponding ^{13}C MAS NMR data were also acquired using a ramped ^1H–^{13}C CPMAS experiment and SPINAL-64 heteronuclear decoupling scheme during acquisition. A Bruker 4.0 mm dual channel (HX) MAS probe was used which implemented spinning frequencies of 8 and 12 kHz to clearly identify the sideband manifold defining the ^{13}C chemical shift anisotropy. All ^{13}C CPMAS data were calibrated against the primary ^{13}C reference of TMS *via* a secondary solid reference of alanine (three ^{13}C shifts of δ_{iso} 20.5, 51.0 and 177.8 ppm). A minimum

Table 5 Crystal data for ketones **7–11**

Parameters	**7**[a]	**8**	**9**	**10**	**11**
Formula	$C_{14}H_{15}NO$	$C_{16}H_{19}NO$	$C_{17}H_{21}NO$	$C_{19}H_{17}NO$	$C_{14}H_{12}F_3NO$
M_r	213.27	241.32	255.36	275.34	267.25
Crystal system	Monoclinic	Orthorhombic	Triclinic	Monoclinic	Monoclinic
Space group	$P2_1/n$	$Pna2_1$	$P\bar{1}$	$P2_1/n$	$P2_1/n$
a/Å	8.3814(2)	9.37(2)	10.4848(6)	9.0485(4)	12.5626(8)
b/Å	10.2345(2)	9.34(2),	12.0004(7)	11.9670(5)	7.4932(4)
c/Å	13.8672(9)	15.72(4)	12.0396(8)	14.4409(6)	13.1887(9)
α/°	90	90	73.685(5)	90	90
β/°	105.897(8)	90	85.342(6)	107.512(5)	98.319(6)
γ/°	90	90	83.541(6)	90	90
V/Å^3	1144.03(8)	1376(5)	1442.66(15)	1491.24(11)	1228.44(13)
Z	4	4	4	4	4
D_{calcd}/g cm^{-3}	1.24	1.16	1.18	1.23	1.44
μ/mm^{-1}	0.078	0.072	0.072	0.075	0.122
T/K	100	100	100	150	150
Reflns, R_{int}	2586, 0.024	3086, 0.056	6618, 0.029	3429, 0.026	2795, 0.034
Reflns, with $F^2 > 2\sigma$	2297	2863	5418	2641	1992
$R(F, F^2 > 2\sigma)$, wR(all)	0.038, 0.100	0.048, 0.135	0.039, 0.106	0.056, 0.114	0.052, 0.102
Crystals from	Ether	Sublimation *in vacuo*	Acetone	Ether	Acetone

[a] A room temperature structure has been reported.[5]

Table 6 Crystal data for the salts of ketones **7–11**

Parameters	**7**-H$^+$·Cl$^-$·H$_2$O[a]	**7**-H$^+$·CF$_3$SO$_3^-$[b]	**8**-H$^+$·BF$_4^-$	**9**-H$^+$·CF$_3$SO$_3^-$[c]	**10**-H$^+$·BF$_4^-$	**11**-H$^+$·CF$_3$SO$_3^-$·H$_2$O
Formula	$C_{14}H_{16}NO{\cdot}Cl{\cdot}H_2O$	$C_{14}H_{16}NO{\cdot}CF_3SO_3$	$C_{16}H_{20}NO{\cdot}BF_4$	$C_{17}H_{22}NO{\cdot}CF_3SO_3$	$C_{19}H_{18}NO{\cdot}BF_4$	$C_{14}H_{13}F_3NO{\cdot}CF_3SO_3{\cdot}H_2O$
M_r	267.74	363.35	329.14	405.43	363.15	435.34
Crystal system	Monoclinic	Monoclinic	Monoclinic	Monoclinic	Orthorhombic	Monoclinic
Space group	$P2_1/c$	$P2_1/c$	$P2_1/n$	$P2_1/c$	$Pbca$	$P2_1/c$
a/Å	11.3796(3)	13.8475(10)	6.2039(2)	21.072(4)	13.6452(5)	10.3782(7)
b/Å	10.5436(2)	7.7466(4)	10.6675(3)	11.828(3)	13.5547(4)	17.4219(8)
c/Å	11.0577(3)	15.6785(9)	23.5777(8)	16.397(4)	18.2545(8)	9.9913(4)
α/°	90	90	90	90	90	90
β/°	97.604(2)	106.669(6)	97.541(3)	112.765(14)	90	103.321(7)
γ/°	90	90	90	90	90	90
V/Å^3	1315.06(6)	1611.17(17)	1546.88(8)	3768.5(15)	3376.3(2)	1757.90(16)
Z	4	4	4	8	8	4
D_{calcd}/g cm^{-3}	1.35	1.49	1.41	1.43	1.43	1.65
μ/mm^{-1}	0.284	0.253	0.12	0.22	0.12	0.27
T/K	150	150	150	100	150	100
Reflns, R_{int}	3007, 0.023	3727, 0.042	3555, 0.024	8602, 0.024	3948, 0.031	4015, 0.027
Reflns, with $F^2 > 2\sigma$	2500	2988	2809	7821	2983	3459
$R(F, F^2 > 2\sigma)$, wR(all)	0.042, 0.104	0.103, 0.225	0.058, 0.142	0.042, 0.088	0.077, 0.166	0.032, 0.078
Crystals from	Acetonitrile	Acetonitrile	Acetonitrile	Acetone	Acetonitrile	Acetone

[a] The positions of the water molecule's hydrogen atoms were constrained to be 0.85 Å from the O atom, and 1.34 Å apart. [b] There is some unresolved disorder in the triflate anion. [c] Crystal was a merohedral twin, twin law (1 0 1, 0 −1 0, 0 0 −1), refined BASF = 0.47.

of 8352 transients were acquired for each spectrum, and a ^{1}H $\pi/2$ pulse width of 3 μs, a ^{1}H–^{13}C Hartmann–Hahn contact period of 1 ms and a recycle delay of 2 s were utilised for all ^{13}C CPMAS NMR measurements. Additional ^{1}H MAS NMR measurements were performed at 14.1 T and at ambient temperatures using a Bruker Avance II+ −600 spectrometer (Larmor frequencies of $\nu_0(^1H)$ = 600.3 MHz). A Bruker 2.5 mm dual channel (HX) MAS probe was used which delivered spinning frequencies of 30 kHz, and all ^{1}H MAS NMR data were acquired using single pulse experiments. An excitation pulse of 2.5 μs and recycle delays of 10s were common to all measurements (although checks for slower relaxing H species were undertaken), and the reported ^{1}H chemical shifts are directly referenced to the primary reference TMS.

Ab initio density functional theory calculations

Ab initio density functional calculations (DFT) calculations were performed using CASTEP 6.01,[29] a DFT code that evokes the Kohn–Sham DFT formalism using a planewave description of the electronic wavefunction under a pseudopotential approximation. The pseudopotentials were generated on-the-fly using the Accelrys' Material Studio 5.5 software.[30] Full details are supplied in the ESI.†

Acknowledgements

We thank the EPSRC for grant (EP/E018203/1) from the Physical Organic Chemistry Initiative and for funding the UK National Crystallography Service including access to Synchrotron facilities at the Diamond Light Source, the EPSRC UK National Mass Spectrometry Facility for data, and the Chemical Database Service[31] for access to the Cambridge Structural Database.[32] We thank Nottingham Trent University for support for diffraction facilities, and the Erasmus program for supporting NM. JVH thanks EPSRC and the University of Warwick for partial funding of the solid state NMR infrastructure at Warwick, and acknowledges additional support for this infrastructure obtained through Birmingham Science City: Innovative Uses for Advanced Materials in the Modern World (West Midlands Centre for Advanced Materials Projects 1 and 2), with support from Advantage West Midlands (AWM) and partial funding by the European Regional Development Fund (ERDF). JVH also acknowledges the facilities of HECToR, the UK's national high-performance computing service, which is provided by UoE HPCx Ltd. at the University of Edinburgh, Cray Inc. and NAG Ltd., and funded by the Office of Science and Technology through EPSRC's High End Computing Programme.

References

1 P. C. Bell and J. D. Wallis, *Chem. Commun.*, 1999, 257–258.
2 J. O'Leary, X. Formosa, W. Skranc and J. D. Wallis, *Org. Biomol. Chem.*, 2005, **3**, 3273–3283.
3 A. Lari, M. B. Pitak, S. J. Coles, G. J. Rees, S. P. Day, M. E. Smith, J. V. Hanna and J. D. Wallis, *Org. Biomol. Chem.*, 2012, **10**, 7763–7779.
4 G. Dyker, M. Hagel, G. Henkel, M. Kockerling, C. Nather, S. Petersen and G. P. Schiemenz, *Z. Naturforsch., B: J. Chem. Sci.*, 2001, **56**, 1109–1116.
5 W. B. Schweizer, G. Procter, M. Kaftory and J. D. Dunitz, *Helv. Chim. Acta*, 1978, **61**, 2783–2808.
6 I. I. Schuster, A. J. Freyer and A. L. Rheingold, *J. Org. Chem.*, 2000, **65**, 5752–5759.
7 (*a*) R. Taylor, O. Kennard and W. Versichel, *J. Am. Chem. Soc.*, 1983, **105**, 5761–5766; (*b*) P. Murray-Rust and J. P. Glusker, *J. Am. Chem. Soc.*, 1984, **106**, 1018–1025.
8 R. J. T. Houk, A. Monzingo and E. V. Anslyn, *Acc. Chem. Res.*, 2008, **41**, 401–410.
9 E. S. Stoyanov, I. V. Stoyanova and C. A. Read, *Chem. – Eur. J.*, 2008, **14**, 7880–7891; T. Steiner and S. A. Mason, *Acta Crystallogr., Sect. B: Struct. Sci.*, 2000, **56**, 254–260.
10 M. Meot-Ner and C. A. Deakyne, *J. Am. Chem. Soc.*, 1985, **107**, 474–479.
11 G. H. Penner, R. Webber and L. A. O'Dell, *Can. J. Chem.*, 2011, **89**, 1036–1046.
12 T. Giavani, K. Johannsen, C. J. H. Jacobsen, N. Blom, H. Bildsoe, J. Skibsted and H. J. Jacobsen, *Solid State Nucl. Magn. Reson.*, 2003, **24**, 218–235.
13 B. C. Chen, W. von Philipsborn and K. Nagarajan, *Helv. Chim. Acta*, 1983, **66**, 1537–1555.
14 G. J. Martin, J. P. Gouesnard, J. Dorie, C. Rabiller and M. L. Martin, *J. Am. Chem. Soc.*, 1977, **99**, 1381–1384.
15 A. Tkatchenko and M. Scheffler, *Phys. Rev. Lett.*, 2009, **102**, 073005.
16 Z. Gu and A. McDermott, *J. Am. Chem. Soc.*, 1993, **115**, 4282–4285.
17 G. J. Rees, S. P. Day, A. Lari, A. P. Howes, D. Iuga, M. B. Pitak, S. J. Coles, T. L. Threlfall, M. E. Light, M. E. Smith, J. D. Wallis and J. V. Hanna, *CrystEngComm*, 2013, **15**, 8823–8839.
18 Z. Gu, R. Zambrano and A. McDermott, *J. Am. Chem. Soc.*, 1994, **116**, 6368–6372.
19 R. Gobetto, C. Nervi, M. R. Chierotti, D. Braga, L. Maini, F. Grepioni, R. K. Harris and P. Hodgkinson, *Chem. – Eur. J.*, 2005, **11**, 7461–7471.
20 P. A. Frey, *Magn. Reson. Chem.*, 2001, **39**, S190–S198.
21 C. Kiefl and A. Mannschreck, *Synthesis*, 1995, 1033–1037.
22 M. Hojo, R. Masuda and E. Okada, *Tetrahedron Lett.*, 1987, **28**, 6199–6200.
23 S. J. Coles and P. A. Gale, *Chem. Sci.*, 2012, **3**, 683–689.
24 *Crystal Clear-SM Expert 2.0 r11*, Rigaku, 2011.
25 *CrysAlisPro, Agilent Technologies, Version 1.171.35.15* (release 03-08-2011 CrysAlis171 .NET).
26 G. M. Sheldrick, *Acta Crystallogr., Sect. A: Found. Crystallogr.*, 2008, **64**, 112–122.
27 L. J. Barbour, X-Seed - A software tool for supramolecular crystallography, *J. Supramol. Chem.*, 2001, **1**, 189–191.
28 C. F. Macrae, P. R. Edgington, P. McCabe, E. Pidcock, G. P. Shields, R. Taylor, M. Towler and J. van de Streek, *J. Appl. Crystallogr.*, 2006, **39**, 453–457.
29 S. J. Clark, M. D. Segall, C. J. Pickard, P. J. Hasnip, M. J. Probert, K. Refson and M. C. Payne, *Z. Kristallogr.*, 2005, **220**, 567–570.
30 Accelrys Inc., 10188 Telesis Court, Suite 100 San Diego, CA 92121, USA.
31 D. A. Fletcher, R. F. McMeeking and D. Parkin, The United Kingdom Chemical Database Service, *J. Chem. Inf. Comput. Sci.*, 1996, **36**, 746–749.
32 F. H. Allen, *Acta Crystallogr., Sect. B: Struct. Sci.*, 2002, **58**, 380–388.

